PAPER

Check for updates

Low-temperature selective catalytic reduction of NOx with NH3 over an activated carbon-carbon nanotube composite material prepared by in situ method†

Pengchen Wang,[a] Lu Yao, ID *[a] Yijuan Pu,[b] Lin Yang,[ab] Xia Jiang ID [ab] and Wenju Jiang*[ab]

Ce-supported activated carbon–carbon nanotube composite (Ce/AC-CNTs) catalyst was prepared by in situ formation of CNTs on AC and then modified by Ce. This Ce/AC-CNTs catalyst was subsequently used for low-temperature selective catalytic reduction of NOx with NH3 (NH3-SCR). The NO conversion of Ce/AC-CNTs was 1.41 times higher than that of Ce/AC at 150 °C with good SO2 tolerance. The catalysts were analyzed by N2 physisorption, SEM, XRD, NH3-TPD, XPS, and Raman technologies. The results showed that the introduction of CNTs could form new mesopores and increase the amount of surface chemisorbed oxygen and acid sites, which all contribute to the high NH3-SCR activity.

1. Introduction

Nitrogen oxides (NOx) originating from fossil fuel combustion have caused serious environmental pollution problems, such as photochemical smog, acid rain, ozone layer depletion, and even global warming.[1,2] Among various denitrification technologies the selective catalytic reduction of NOx with NH3 (NH3-SCR) is the most successful and widely applied technology.[3,4] The V2O5–WO3(MoO3)/TiO2 catalyst is used as a typical commercial NH3-SCR catalyst which works at relatively high temperatures (300–400 °C).[5,6] However, some inevitable disadvantages of the commercial catalysts, such as the narrow operation temperature window and the poor low-temperature catalytic activity, are still observed.[7,8] Therefore, developing an efficient catalyst for low temperature NH3-SCR reaction is highly desirable.

Activated carbon (AC) have been widely used as the support for NH3-SCR catalysts due to its low price and developed porous structure.[9] Wang et al. found that the CeMn/AC catalyst showed 44% NO removal efficiency at 160 °C.[10] Jing et al. reported that the V2O5/AC exhibited 60% NO conversion at 150 °C.[11] However, the AC-catalysts were easily deactivation in the presence of SO2.[12] Therefore, further efforts should be carried out to improve SO2 resistance of SCR catalysts.

Carbon nanotubes (CNTs) were used as support for NH3–SCR reaction in recent years due to their high adsorbability for NOx and NH3.[13] Besides, NO could even be decomposed directly over CNTs,[14] and importantly, the CNTs-catalyst presented good SO2 and water resistance.[15] Luo et al. found that NO can be 100% decomposed at 600 °C on CNTs.[16] Bai et al. reported that the NO conversion of V2O5/CNTs (50%) was higher than that on V2O5/AC (38%) at 250 °C, and V2O5/CNTs also had a better SO2 resistance compared with V2O5/AC.[17] Cai et al. found that the catalytic activity of Fe@Mn@CNTs is barely affected by the SO2 and exhibits an over 85% NO conversion temperature window from 150 to 270 °C.[18] Santillan-Jimenez et al. investigated the existence of H2O and noted slight inhibitory effects on the catalytic activity of the SCR catalyst when CNTs were used as the support.[19] Thus, considering of the cost and catalytic performance, an activated carbon-carbon nanotubes composite (AC-CNTs) was used for NH3-SCR reaction.

Due to the low dispersion and self-aggregation property of carbon nanotubes, it is difficult to get carbon nanotubes into AC by mechanical mixing method.[20] Su et al. successfully prepared AC-CNT (CNF) composite by treating the Fe/AC catalyst in flowing C2H4/H2.[21] Chen et al. also found that the CNTs were successfully grew on Fe-deposited Si substrate via the chemical vapor deposition method using a CH4–CO2 gas mixture.[22] However, the use of AC-CNTs composites in the NH3-SCR reaction has not been reported.

In this work, an AC-CNTs composite was prepared via CH4 decomposition on AC. Then the Ce/AC-CNTs catalysts were obtained by an impregnation method. This work aims to combine the advantages of CNTs and AC and used the Ce/AC-CNTs catalyst for NH3-SCR reaction at low temperature. The

*a*College of Architecture and Environment, Sichuan University, Chengdu 610065, P. R. China. E-mail: yaolu@scu.edu.cn; wenjujiang@scu.edu.cn; Fax: +86-28-8540-5613; Tel: +86-28-8540-7800

*b*National Engineering Research Center for Flue Gas Desulfurization, Chengdu 610065, P. R. China

physicochemical properties of catalysts were also comprehensively discussed in the present work.

2. Materials and methods

2.1 Materials

The AC (C 78.68%, N 0.27%, O 18.59%, and H 2.46%) was used as the precursor to prepare activated carbon-CNTs (AC-CNTs) bought from Xinhua Activated Carbon Co., Ltd. The agents used in this study, such as $Ni(NO_3)_2 \cdot 6H_2O$ and $Ce(NO_3)_3 \cdot 6H_2O$, were of analytical reagent grade (AR) and purchased from Chengdu Chron Chemicals Co., Ltd.

2.2 Preparation of catalysts

The AC-CNTs were prepared *via in situ* formation of CNTs (by methane decomposition) on AC. First, AC was impregnated with a certain amount of $Ni(NO_3)_2$ solution for 24 h at 25 °C and then dried at 80 °C for 12 h to obtain the Ni/AC precursor, which was the catalyst of methane decomposition. Subsequently, the obtained sample was pretreated at 750 °C under N_2 flow for 2 h, and then, cooled to 650 °C (with switching to CH_4 atmosphere) for 30 min to produce CNTs on AC (AC-CNTs). The obtained sample was named AC-CNTs. The AC and AC-CNTs impregnated with the $Ce(NO_3)_3$ solution and calcined at 450 °C for 6 h under N_2 atmosphere were donated as Ce/AC and Ce/AC-CNTs, respectively.

2.3 Denitrification test

NH_3-SCR experiments of the prepared samples were performed in a fixed-bed quartz tube reactor with an internal diameter of 10 mm. The reaction temperature and space velocity (GHSV) was 150 °C and 50 000 h^{-1}, respectively. The total flow rate of gas was 500 mL min^{-1}, and the typical reactant gas contained 500 ppm of NO, 550 ppm of NH_3, 5 vol% of O_2, 50 ppm (142.8 mg m^{-3}) of SO_2 (when used), 10 vol% of H_2O (when used), and balance of N_2. A flue gas analyzer (Gasboard-3000, Wuhan Cubic Optoelectronics Co., Ltd., CN) was used to determine the inlet and outlet NO concentrations online. The NO reduction with NH_3 of all samples was beginning (was started) at the NO saturated sample under the same denitrification condition to eliminate the adsorption effect of NO.

2.4 Characterization of adsorbents

N_2 adsorption–desorption experiments of the prepared samples were measured at 77 K using the ASAP 2460 instrument (Micromeritics Instrument Co., Ltd., USA). The specific surface area (S_{BET}), total pore volume (V_{tot}), mesopore volume (V_{mes}), micropore volume (V_{mic}), and pore size distribution were obtained from the N_2 adsorption–desorption isotherms by using the Brunauer–Emmett–Teller (BET) equation, N_2 adsorption amount at the maximum relative pressure, Barrett–Joyner–Halenda method, *t*-plot method, and density functional theory method, respectively. The surface morphology of samples was observed microscopically *via* scanning electron microscopy (SEM, JSM-7500F, Jeol Co., Ltd., Japan).

The crystal structure of AC was analyzed by X-ray diffraction using an X'Pert PRO MPD diffractometer (Panalytical Co., Ltd., Netherlands). The crystalline phases were identified by comparison with the reference data from the International Center for Diffraction Data (JCPDs).

The NH_3-temperature-programming desorption (NH_3-TPD) was conducted on a TP-5076 chemisorption analyzer (Tianjin First Industry and Trade Development Co. Ltd., CN). The samples were pretreated at 400 °C in a He flow for 1 h. Subsequently, the samples were cooled down to 30 °C and saturated with NH_3 until adsorption equilibrium was reached, followed by blowing with He at the same temperature to avoid NH_3 physisorption. The saturated samples were then heated from 30 °C to 800 °C at a rate of 10 °C min^{-1} in He.

The surface chemistry was determined by X-ray photoelectron spectroscopy using an XSAM-800 spectrometer (Kratos Co., Ltd., UK) with light as the mono Al $K\alpha$ (1486.6 eV). Raman spectra were collected by a Raman spectrometer (LabRAM-HR, Horiba Co., Ltd., Japan). The wavelength and power were 532 nm and 5 mW, respectively, while the spectral resolution was ± 1 cm^{-1}.

3. Results and discussion

3.1 Catalyst characterization

3.1.1 Textural properties. Fig. 1 shows loose and porous structures of the AC surface. After the introduction of CNTs, distinct CNTs were observed on the surface of AC-CNTs with a length distribution of approximately 100–300 nm and diameter of 10–30 nm.

N_2 adsorption–desorption isotherms and textural properties of the prepared samples are shown in Fig. S1 (seen in ESI†) and Table 1, respectively. The BET surface area of the catalysts varied as follows: AC (803 m^2 g^{-1}) > AC-CNTs (774 m^2 g^{-1}) > Ce/AC (700 m^2 g^{-1}) > Ce/AC-CNTs (599 m^2 g^{-1}). Notably, the V_{mic} evidently decreased after the introduction of CNTs. The V_{mic} of AC and Ce/AC was 0.28 and 0.24 cm^3 g^{-1} while that of AC-CNTs and Ce/AC-CNTs decreased to 0.24 and 0.17 cm^3 g^{-1}, respectively, after CNTs introduction. However, the V_{mes} of the catalyst displayed an opposite trend to that of V_{mic}. The V_{mes} of AC and Ce/AC was 0.24 and 0.19 cm^3 g^{-1} while that of AC-CNTs and Ce/AC-CNTs increased to 0.31 and 0.22 cm^3 g^{-1}, respectively, after CNTs introduction. Furthermore, the V_{mic}/V_{tot} and average pore size decreased, while the V_{mes}/V_{tot} increased after CNTs introduction. These results suggested that pore blockage occurred to
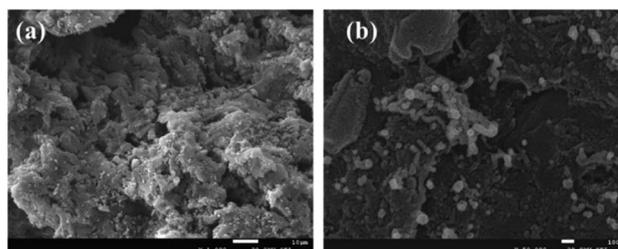

Fig. 1 SEM images of (a) AC and (b) AC-CNTs.

Table 1 Textural structure parameters of prepared samples[a]

Catalyst	S_{BET} (m² g⁻¹)	V_{tot} (cm³ g⁻¹)	V_{mic} (cm³ g⁻¹)	V_{mes} (cm³ g⁻¹)	V_{mic}/V_{tot} (%)	V_{mes}/V_{tot} (%)	D_{mean} (nm)
AC	803	0.57	0.28	0.24	48.2	41.4	6.42
AC-CNTs	774	0.58	0.24	0.31	41.5	53.6	3.00
Ce/AC	700	0.48	0.24	0.19	50.6	39.8	6.32
Ce/AC-CNTs	599	0.43	0.17	0.22	39.5	51.1	5.22

[a] S_{BET}, BET surface area; V_{tot}, total pore volume; V_{mic}, micropore volume; V_{mes}, mesopore volume; D_{mean}, average pore diameter.

a considerable extent upon the loading of Ce species and formation of CNTs due to the obvious decrease of the S_{BET} and V_{mic} after the introduction of Ce and CNTs.

Interestingly, the V_{mes} of AC increased from 0.28 cm³ g⁻¹ to 0.31 cm³ g⁻¹ for AC after CNT introduction and decreased to 0.22 cm³ g⁻¹ after the further introduction of Ce. This result inferred that the *in situ* formation of CNTs on AC may form some new mesopores on AC-CNTs. Meanwhile, a certain extent of pore blockage occurred on Ce/AC-CNTs after Ce introduction.

Raman spectra were performed to further study the structure of Ce/AC and Ce/AC-CNTs catalysts, and the results are shown in Fig. 2. The two main peaks were at approximately 1323 cm⁻¹ (D-band) and 1590 cm⁻¹ (G-band).[23] The D-band of the catalyst was mainly derived from the disordered carbon or amorphous carbon, whereas the G-band was assigned to the well-ordered carbon. The intensity ratio (I_D/I_G) of D-band to G-band is an index of the integrity of catalysts.[24] As shown in Fig. 2, the I_D/I_G of Ce/AC (1.2) was lower than that of Ce/AC-CNTs (1.3). The increased I_D/I_G of Ce/AC-CNTs was attributed to the generation of new defects and surface functional groups during the CNTs formation (methane decomposition on AC). This result suggested that the introduction of CNTs favored the formation of disordered or defected carbon.

3.1.2 Surface acidity. The surface acidity of catalysts is generally one of the key factors for their denitrification performance in the NH₃-SCR reaction. The adsorption and activation of NH₃ species over the catalysts were highly dependent on the surface acidity properties of the catalysts. The NH₃-TPD

experiments were conducted to measure the number of acid sites and strength of acid on the surface of Ce/AC and Ce/AC-CNTs catalysts. The NH₃ desorption temperature and integral area of desorption peaks in NH₃-TPD profiles could represent the acid strength and the number of acid sites, respectively. As shown in Fig. S3 (seen in ESI†), the Ce/AC and Ce/AC-CNTs catalysts exhibited three desorption peaks during 50 °C-650 °C with the increase in desorption temperature and are denoted as I, II, and III. In the NH₃-TPD curves of Ce/AC, the low-temperature desorption peak I centered at approximately 124 °C was attributed to NH₃ species desorbed from the weak acid sites. Peak II centered at 179 °C was assigned to desorption of NH₃ species from medium to strong acid sites. Peak III centred at 377 °C was related to strong acid sites.[25] As reported, the NH_4^+ ions adsorbed on the Lewis acid sites were more thermally stable than those of Brønsted acid sites. Thus, the desorption peak at low temperature of catalysts was ascribed to the NH_4^+ ions adsorbed on the Brønsted acid sites, while the desorption peak at high temperature was due to NH₃ molecules originating from the Lewis acid sites.[26]

Ce/AC and Ce/AC-CNTs presented three strong NH₃ desorption peaks (Fig. S3 in ESI†). As shown in Table 2, the quantitative data (from the area of the desorption peak) of NH₃-TPD suggested that the relative amount of acid sites on Ce/AC-CNTs (19.14 mmol g⁻¹) was higher than that of Ce/AC (15.80 mmol g⁻¹). This result implied that the Ce/AC-CNTs catalyst possessed more acid sites than that of Ce/AC. Moreover, the curve of NH₃ desorption peaks for Ce/AC-CNTs shifted toward the high temperature region (from 377 °C to 470 °C). This result demonstrated that the strength of acid sites on Ce/AC-CNTs was stronger than that of Ce/AC. Thus, Lewis acidity was strengthened on Ce/AC-CNTs. As reported, the CNTs could supply strong acid sites, and CeO₂ supported on CNTs could significantly increase the acidity of CNTs and in favor of the NH₃-SCR reaction.[27]

3.1.3 XPS. The binding energy and surface atomic composition of Ce/AC and Ce/AC-CNTs were estimated by XPS analysis. Table 3 shows that the relative content of total oxygen of Ce/AC-CNTs was 14.3%, which was higher than that of Ce/AC (11.6%). The ratios of O/C for Ce/AC-CNTs and Ce/AC were 0.17 and 0.13, respectively. Thus, CNTs introduction could promote the formation of surface total oxygen, which could contribute to the high catalytic activity of Ce/AC-CNTs for NH₃-SCR reaction; this outcome was in good agreement with the results of Wang.[24]

The O 1s spectra of Ce/AC and Ce/AC-CNTs are exhibited in Fig. S4 (seen in ESI†). Three distinct peaks were observed for Ce/
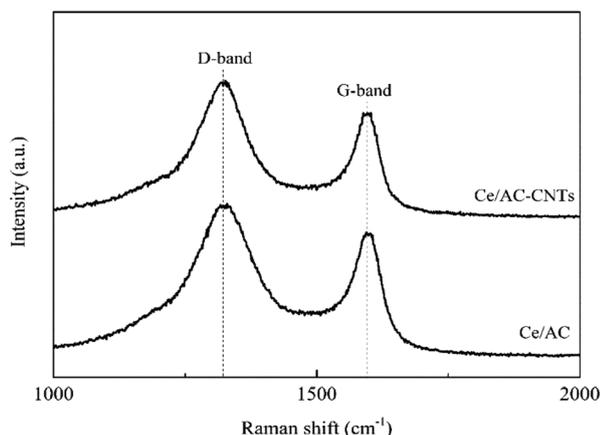

Fig. 2 Comparison of the Raman spectra of Ce/AC and Ce/AC-CNTs.

Table 2 Deconvolution of the NH_3-TPD profiles of Ce/AC and Ce/AC-CNTs catalysts

Catalyst	Peak temp. (°C)			Relative amount of acid sites (%)			Total desorption amount (mmol g^{-1})
	Peak I	Peak II	Peak III	S I	S II	S III	
Ce/AC	124	179	377	24.9	36.1	39.0	15.80
Ce/AC-CNTs	123	179	470	25.4	36.1	38.5	19.14

Table 3 XPS results of the catalysts

Sample	Ce/AC	Ce/AC-CNTs
C (%)	87	84.2
O (%)	11.6	14.3
O/C	0.13	0.17
Ce (%)	1.5	1.5
$(O_\beta)/(O_\alpha + O_\beta + O_\gamma)$ (%)	38.6	42.1

AC and Ce/AC-CNTs. One major peak that appearing at approximately 529.6 eV is assigned to lattice oxygen (O^{2-}) (denoted as O_α). Meanwhile, two peaks that appeared at relatively high binding energy located at approximately 532.3 and 533.8 eV could be assigned to chemisorbed oxygen (denoted as O_β) and –O– oxygen (denoted as O_γ).[28] The O_β, which was the most active oxygen, generally had a strong migration capability, and usually adsorbed on the defective sites of catalysts.[29]

In this study, the relative content of chemisorbed oxygen of Ce/AC-CNTs calculated by $O_\beta/(O_\alpha + O_\beta + O_\gamma)$ was 42.1%, which was higher than that of Ce/AC (38.6%). As reported, metal oxides, such as CeO_2 and MnO_2, could increase the electrochemical active surface area of the catalyst.[30] Thus, the introduction of CNTs increased the chemisorbed oxygen and promotion of the electron transfer on the surface of catalyst, these conditions were beneficial to the catalytic activity of Ce/AC-CNTs for the NH_3-SCR reaction.[31–34]

3.2 Catalytic activity

Fig. 3 shows the NO conversions of NH_3-SCR reaction over different catalysts. The results showed that the NO conversion

(9.4%) over the AC was quite low at 150 °C, whereas the NO conversion over AC-CNTs (<1%) was even lower than that of AC. Moreover, the nickel species on AC-CNTs and Ce/AC-CNTs are mainly in bulk, instead of surface (Table S1 in ESI†), which indicated that the Ni species on catalyst has no obvious effect on denitrification performance. For the Ce-added AC (Ce/AC catalyst), the NO conversion (29.4%) was much higher than that on non-promoted AC (9.4%) due to the presence of the active ceria species. Interesting, compared with Ce/AC, NO conversion evidently improved over Ce/AC-CNTs (41.4%), which was 1.41 times as that of Ce/AC. The effluent gases from stationary sources always contain trace amounts of SO_2 and water vapor, which could have inhibitory effects on the NO_x removal, especially at low temperature.[35] Thus, SO_2 and water vapor deactivation experiments were performed to clarify the impacts of SO_2 and water vapor on the Ce/AC-CNTs (Fig. 3b). As shown in Fig. 3b, with the absence of SO_2, the catalyst maintained NO conversion at approximately 41.4%. When 50 ppm of SO_2 was added into the inlet gas, only a slight inhibition effect on NO conversion (decreased by 4.8%) was observed on Ce/AC-CNTs, whereas that of Ce/AC exhibited serious decrease (16.3%) in its NO conversion (Fig. S6 and S7 in ESI†). After the removal of the SO_2 gas, the catalytic activity of Ce/AC-CNTs catalyst was restored to approximately 41.4% as before. Moreover, when H_2O was added into the inlet gas, the NO conversion of Ce/AC-CNTs decreased by 21.7%, while the NO conversion of Ce/AC decreased by 30.6%.

Furthermore, the NO conversion was rapidly restored to 39.4% when the water vapor supply was turned off. The results indicated the reversible inhibitory effect of water of Ce/AC-CNTs catalyst. The high NO conversion and good SO_2 tolerance of Ce/AC-CNTs suggested that a significant synergistic effect between CeO_2 and CNTs contribute to the NH_3-SCR reaction.
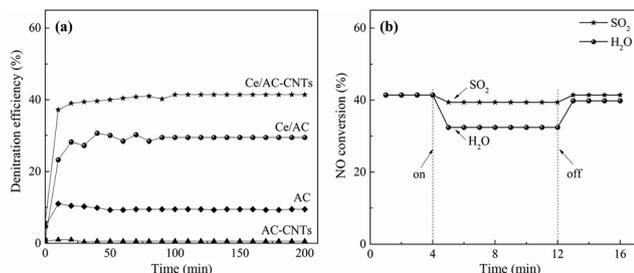

Fig. 3 Variation of (a) NO conversion of AC, AC-CNTs, Ce/AC and Ce/AC-CNTs, and (b) SO_2 tolerance and water-resistance of Ce/AC-CNTs over time. Reaction conditions: [NO] = 500 ppm, [NH_3/NO] = 1.1, [O_2%] = 5 vol%, [SO_2] = 50 ppm (when used), [H_2O%] = 10 vol% (when used), N_2 balance, reaction temperature = 150 °C and GHSV = 50 000 h^{-1}.

Table 4 Comparison of NO removal efficiency of various catalysts

Sample	Temperature (°C)	NO removal efficiency (%)	Reference
Ce/AC-CNTs	150	41	This work
Mn-CeO$_x$/AC	220	35	3
V$_2$O$_5$/AC	150	30	36
V–Zr/AC	150	40	16
Mn@CNTs	150	59	37
Fe@Mn@CNTs	90	40	37
Fe-Cu-O/CNTs-TiO$_2$	250	12	38
V$_2$O$_5$/CNT	270	38	32

The comparison of NO removal efficiency with those of literatures have been studied. As it was shown in Table 4, at 150 °C, NO removal efficiency Ce/AC-CNTs (the present work) was 41%, which was higher than reported M/AC (M = metal) catalysts, and even higher than many M/CNTs catalysts. This indicated that the Ce/AC-CNTs catalyst in the present work is competitive for NH_3-SCR reaction.

4.   Further discussion

A CNT-promoted-Ce/AC-CNTs catalyst (Ce/AC-CNTs) was prepared by *in situ* formation of CNTs on AC (*via* decomposition of methane) and used for NH_3-SCR reaction. The catalytic activity of Ce/AC-CNTs catalyst (41.4%) was much higher than that of Ce/AC (29.4%). Although pore blockage occurred to a large extent upon the introduction of CNTs with the decrease in S_{BET} and V_{mic}, the V_{mes} of AC-CNTs and Ce/AC-CNTs increased to 0.07 cm^3 g^{-1} and 0.03 cm^3 g^{-1} compared with that of AC and Ce/AC, respectively, after the introduction of CNTs. Thus, the *in situ* formation of CNTs on AC formed some new mesopores on AC-CNTs and Ce/AC-CNTs.

CNTs introduction could facilitate the formation of surface total oxygen amount (increasing from 11.6% of Ce/AC to 14.3% of Ce/AC-CNTs) and chemisorbed oxygen (increasing from 38.6% of Ce/AC to 42.1% of Ce/AC-CNTs). The increased amount of chemisorbed oxygen contributes to the high catalytic activity.

CNTs introduction increased the number of acid sites and strengthened the acidity of Ce/AC-CNTs, which enhanced the NH_3 adsorption on catalysts and then improved the SCR catalytic activity. The cost of the AC-CNTs in this work was about 369 Chinese Yuan per kilogram (in laboratory). However, the commercial CNTs (Chengdu Branch Chinese Academy of Science) was 30 000 Chinese Yuan per kilogram, which indicated that the AC-CNTs prepared in this work greatly reduced the cost of catalyst compared to CNTs.

5.   Conclusions

Ce/AC-CNTs catalyst was prepared by *in situ* formation of CNTs on AC and then modified by Ce, and used for NH_3-SCR reaction. The NO conversion of Ce/AC-CNTs was 1.41 times higher than that of Ce/AC at 150 °C with good SO_2 tolerance. CNTs introduction could form new mesopores and provide several acid sites, high surface total oxygen, and high surface chemisorption oxygen concentration on Ce/AC-CNTs, resulting in an enhancement of NH_3-SCR.

Conflicts of interest

There are no conflicts to declare.

Acknowledgements

Notes and references

1 H. Jiang, Y. Niu, Q. Wang, Y. Chen and M. Zhang, *Catal. Commun.*, 2018, **113**, 46–50.
2 Z. Song, X. Wu, Q. Zhang, P. Ning, J. Fan, X. Liu, Q. Liu and Z. Huang, *RSC Adv.*, 2016, **6**, 69431–69441.
3 B. Shen, J. Chen, S. Yue and G. Li, *Fuel*, 2015, **156**, 47–53.
4 B. Samojeden and T. Grzybek, *Energy*, 2016, **116**, 1484–1491.
5 G. Ramis, G. Busca, F. Bregani and P. Forzatti, *Appl. Catal.*, 1990, **64**, 259–278.
6 H. Xu, Q. Lin, Y. Wang, L. Lan, S. Liu, C. Lin, Q. Wang, J. Wang and Y. Chen, *RSC Adv.*, 2017, 7, 47570–47582.
7 S. Zhan, Q. Shi, Y. Zhang, Y. Li and Y. Tian, *RSC Adv.*, 2016, **6**, 59185–59194.
8 B. Huang, R. Huang, D. Jin and D. Ye, *Catal. Today*, 2007, **126**, 279–283.
9 Y. Fu, Y. Zhang, G. Li, J. Zhang and F. Tian, *RSC Adv.*, 2016, **6**, 8539–8548.
10 Y. Wang, X. Li, L. Zhan, C. Li, W. Qiao and L. Ling, *Ind. Eng. Chem. Res.*, 2015, **54**, 2274–2278.
11 W. Jing, Q. Guo, Y. Hou, G. Ma, X. Han and Z. Huang, *Catal. Commun.*, 2014, **56**, 23–26.
12 W. Tian, H. Yang, X. Fan and X. Zhang, *J. Hazard. Mater.*, 2011, **188**, 105–109.
13 M. Zheng, P. Li, G. Fu, Y. Chen, Y. Zhou, Y. Tang and T. Lu, *Appl. Catal., B*, 2013, **129**, 394–402.
14 S. J. Wang, W. X. Zhu, D. W. Liao, C. F. Ng and C. T. Au, *Catal. Today*, 2004, **93–95**, 711–714.
15 J. Lilong, Y. Wang, L. Xian, Y. Cao and K. Wei, *Chin. J. Catal.*, 2013, **34**, 2271–2276.
16 J. Z. Luo, L. Z. Gao, Y. L. Leung and C. T. Au, *Catal. Lett.*, 2000, **66**, 91–97.
17 S. Bai, S. Jiang, H. Li and Y. Guan, *Chin. J. Chem. Eng.*, 2015, **23**, 516–519.
18 S. Cai, H. Hu, H. Li, L. Shi and D. Zhang, *Nanoscale*, 2016, **8**, 3588–3598.
19 E. Santillan-Jimenez, V. Miljković-Kocić, M. Crocker and K. Wilson, *Appl. Catal., B*, 2011, **102**, 1–8.
20 K. Lota, V. Khomenko and E. Frackowiak, *J. Phys. Chem. Solids*, 2004, **65**, 295–301.
21 D. Su, X. Chen, G. Weinberg, A. Klein-Hofmann, O. Timpe, S. B. Abd Hamid and R. Schlogl, *Angew. Chem.*, 2005, **44**, 5488–5492.
22 M. Chen, C.-M. Chen, S.-C. Shi and C.-F. Chen, *Jpn. J. Appl. Phys.*, 2003, **42**, 614–619.
23 J. Wei, B. Jiang, X. Zhang, H. Zhu and D. Wu, *Chem. Phys. Lett.*, 2003, **376**, 753–757.
24 L. Wang, B. Huang, S. U. Yanxia, G. Zhou, K. Wang, H. Luo and Y. E. Daiqi, *Chem. Eng. J.*, 2012, **192**, 232–241.
25 X. Yao, L. Zhang, L. Li, L. Liu, Y. Cao, X. Dong, F. Gao, Y. Deng, C. Tang, Z. Chen, L. Dong and Y. Chen, *Appl. Catal., B*, 2014, **150**, 315–329.
26 F. Cheng, Z. Dengsong, C. Sixiang, Z. Lei, H. Lei, L. Hongrui, M. Phornphimon, S. Liyi, G. Ruihua and Z. Jianping, *Nanoscale*, 2013, **5**, 9199–9207.

27 N. Zhu, Z. Lian, Y. Zhang, W. Shan and H. He, *Chin. Chem. Lett.*, 2019, **30**, 867–870.

28 J. Guo, J. Liang, Y. Chu, M. Sun, H. Yin and J. Li, *Appl. Catal., A*, 2012, **421–422**, 142–147.

29 Z. Wu, R. Jin, Y. Liu and H. Wang, *Catal. Commun.*, 2008, **9**, 2217–2220.

30 C. Zhou, H. Wang, F. Peng, J. Liang, H. Yu and J. Yang, *Langmuir*, 2009, **25**, 7711–7717.

31 X. Chen, P. Wang, P. Fang, T. Ren, Y. Liu, C. Cen, H. Wang and Z. Wu, *Fuel Process. Technol.*, 2017, **167**, 221–228.

32 B. Huang, R. Huang, D. Jin and D. Ye, *Catal. Today*, 2007, **126**, 279–283.

33 Z. Liu, Y. Yi, J. Li, S. I. Woo, B. Wang, X. Cao and Z. Li, *Chem. Commun.*, 2013, **49**, 7726–7728.

34 T. Gu, Y. Liu, X. Weng, H. Wang and Z. Wu, *Catal. Commun.*, 2010, **12**, 310–313.

35 F. Cheng, D. Zhang, L. Shi, R. Gao, H. Li, L. Ye and J. Zhang, *Catal. Sci. Technol.*, 2013, **3**, 803–811.

36 A. Boyano, M. J. Lázaro, C. Cristiani, F. J. Maldonado-Hodar, P. Forzatti and R. Moliner, *Chem. Eng. J.*, 2009, **149**, 173–182.

37 S. Cai, H. Hu, H. Li, L. Shi and D. Zhang, *Nanoscale*, 2016, **8**, 3588.

38 Z. Ma, H. Yang, Q. Li, J. Zheng and X. Zhang, *Appl. Catal., A*, 2012, **427–428**, 43–48.